Published in final edited form as:
Biochemistry. 2007 July 31; 46(30): 8709–8716. doi:10.1021/bi700906g.

A Mn(IV)/Fe(IV) Intermediate in Assembly of the Mn(IV)/Fe(III) Cofactor of *Chlamydia trachomatis* Ribonucleotide Reductase†

Wei Jiang[a], **Lee M. Hoffart**[a], **Carsten Krebs**[a,b*], and **J. Martin Bollinger Jr.**[a,b*]

a*Department of Biochemistry and Molecular Biology, The Pennsylvania State University, University Park, Pennsylvania 16802*

b*Department of Chemistry, The Pennsylvania State University, University Park, Pennsylvania 16802*

Abstract

We recently showed that the class I*c* ribonucleotide reductase from the human pathogen, *Chlamydia trachomatis*, uses a Mn^{IV}/Fe^{III} cofactor to generate protein and substrate radicals in its catalytic mechanism [Jiang, W., Yun, D., Saleh, L., Barr, E. W., Xing, G., Hoffart, L. M., Maslak, M.-A., Krebs, C., and Bollinger, J. M., Jr. (2007) *Science 316*, 1188-1191]. Here, we have dissected the mechanism of formation of this novel heterobinuclear redox cofactor from the Mn^{II}/Fe^{II} cluster and O_2. An intermediate with a $g = 2$ EPR signal that shows hyperfine coupling to both ^{55}Mn and ^{57}Fe accumulates almost quantitatively in a second order reaction between O_2 and the reduced R2 complex. The otherwise slow decay of the intermediate to the active Mn^{IV}/Fe^{III}-R2 complex is accelerated by the presence of the one-electron reductant, ascorbate, implying that the intermediate is more oxidized than Mn^{IV}/Fe^{III}. Mössbauer spectra show that the intermediate contains a high-spin Fe^{IV} center. Its chemical and spectroscopic properties establish that the intermediate is a Mn^{IV}/Fe^{IV}-R2 complex with an $S = 1/2$ electronic ground state arising from antiferromagnetic coupling between the Mn^{IV} ($S_{Mn} = 3/2$) and high-spin Fe^{IV} ($S_{Fe} = 2$) sites.

A conventional class I ribonucleotide reductase (RNR[1]), such as the RNR from *Escherichia coli* or *Homo sapiens*, activates O_2 at a carboxylate-bridged $Fe_2^{II/II}$ cluster in its R2 subunit to oxidize a nearby tyrosine (Y) residue to a stable tyrosyl radical (Y•) (1). The Y• in R2 oxidizes a cysteine residue in the R1 subunit by a long-distance (~ 35 Å), inter-subunit, proton-coupled electron transfer (PCET), generating a transient cysteine thiyl radical (C•) (2,3). The C• in R1 initiates reduction of the ribonucleoside diphosphate (NDP) substrate by abstracting the hydrogen atom from C3' (4,5). After reduction of the substrate 3' radical to the 2'-deoxy (product) 3' radical by two additional cysteine residues in R1 (which become oxidized to a disulfide), the hydrogen originally abstracted from C3' is returned to this position, regenerating the C• and yielding the 2'-deoxyribonucleoside diphosphate (dNDP) product. The C• then re-oxidizes the Y in R2 back to the stable Y•.

†This work was supported by the National Institutes of Health (GM-55365 to JMB), the Beckman Foundation (Young Investigator Award to CK), and the Dreyfus Foundation (Teacher Scholar Award to CK).

Please send correspondence to: J. Martin Bollinger, Jr. Department of Biochemistry and Molecular Biology 208 Althouse Laboratory University Park, PA 16802 Phone: 814-863-5707 Fax: 814-863-7024 jmb21@psu.edu. Carsten Krebs Department of Biochemistry and Molecular Biology 306 South Frear Laboratory University Park, PA 16802 Phone: 814-865-6089 Fax: 814-863-7024 ckrebs@psu.edu.

Supporting Information Available. Calculated energies and spin expectation values of the ^{55}Mn hyperfine interaction in low magnetic fields, EPR spectrum of the O_2-reactive Mn^{II}/Fe^{II}-R2 complex, analysis proving the applicability of the pseudo-first-order approximation in analysis of the [O_2]-dependent stopped-flow data, and a comparison of the 4.2-K/53-mT Mössbauer spectra of the Mn^{II}/Fe^{II}-R2 reactant complex and samples frozen at various times after reacting this complex with O_2. This material is available free of charge at the journal website http://pubs.acs.org.

[1]Abbreviations: *Ct*, *Chlamydia trachomatis*; EPR, electron paramagnetic resonance; PCET, proton-coupled electron transfer; RNR, ribonucleotide reductase; NDP, ribonucleoside diphosphate ; dNDP,: 2′-deoxyribonucleoside 5′-diphosphate.

When McClarty and co-workers identified the genes encoding the class I RNR subunits from several species of chlamydiae, they noted that the R2 proteins had phenylalanine (F) residues at the position aligning with the Y•-harboring tyrosine residues of the other R2s (6). They found that the *Chlamydia trachomatis* (*Ct*) RNR was, nevertheless, catalytically active. Subsequent biochemical and structural characterization of the *Ct* R2 confirmed the absence of a Y• and location of F at the site normally harboring the Y• (7). Analysis of genome sequences suggested that Y•-less R2 subunits might also be present in other bacteria (including the important human pathogen, *Mycobacterium tuberculosis*) and archaea, and a new sub-classification of these RNRs as class I*c* was proposed. It was further suggested that a $Fe_2^{III/IV}$ cluster, formed by reaction of O_2 with the $Fe_2^{II/II}$ form of R2 and similar to the intermediate, cluster **X**, which had previously been shown to generate the Y•s in the R2 proteins from *E. coli* and *Mus musculus* (8,9), directly generates the C• in these class I*c* RNRs. Two subsequent studies on *Ct* RNR provided support for this hypothesis by showing that the oxidized diiron cluster could be stabilized for several minutes (10) and even induced to accumulate from $Fe_2^{III/III}$-R2 (11) in a complete RNR reaction solution (containing R1, R2, CDP, ATP, Mg^{2+}, and DTT). However, the relatively meager R2 activity (e.g., < 3% that of *E. coli* R2) and marked variation thereof (230 U/mg in (10) but only < 75 U/mg in (11)) reported by these authors suggested that another, minor form of the protein, present in varying amounts in different preparations, might be responsible for the observed activity. Indeed, we recently demonstrated that a Mn^{IV}/Fe^{III} cluster can be assembled in *Ct* R2 and that this heterodinuclear form exhibits much greater activity than had been observed in the previous studies (12). Importantly, the reduction of the cofactor to the Mn^{III}/Fe^{III} oxidation state and formation of the well-characterized, nitrogen-centered free radical upon incubation of the enzyme with the radical-trapping mechanism-based inactivator, 2'-azido-2'-deoxyadenosine-5'-diphosphate, established that the Mn^{IV}/Fe^{III} cluster is the radical-initiating cofactor of *Ct* RNR. Additional experiments showed that the active cofactor forms by reaction of the reduced (Mn^{II}/Fe^{II}) cluster with O_2, but the activation process was not studied in detail (12). In this work, we have examined the mechanism of activation of *Ct* R2 by stopped-flow absorption and freeze-quench EPR and Mössbauer spectroscopies. The results show that the activation mechanism entails (1) the rapid formation of a Mn^{IV}/Fe^{IV}-R2 intermediate in a bimolecular reaction between the reduced complex and O_2 and (2) the slow decay of the intermediate by reduction of the iron site to Fe^{III}. Kinetic characteristics of the decay step suggest that it may be mediated by the protein, perhaps by the same residues required for the intra-subunit radical transfer that initiates turnover (2).

MATERIAL AND METHODS

Expression and Purification of Ct R2

The protein used throughout this study has an additional 20 amino acids ($MGS_2H_6S_2GLVPRGSH$) appended to the N-terminal methionine residue of *Ct* R2. The appendage contains a His_6 element to permit purification of the protein by metal-ion-affinity chromatography. Preparation of the plasmid that directs over-expression of this protein in *E. coli*, growth of the over-expression strain, and purification of the metal-depleted form of the R2 protein have been described (12).

Preparation of Mn^{II}/Fe^{II}-R2 Complex

In an MBraun anoxic chamber, Mn^{II} and Fe^{II} (natural abundance Fe^{II}, which contains 91.8% $^{56}Fe^{II}$ and is hereafter referred to as $^{56}Fe^{II}$, or ~95% enriched $^{57}Fe^{II}$, which is hereafter referred to as $^{57}Fe^{II}$) were added to the metal-depleted R2 to form the O_2-reactive Mn^{II}/Fe^{II}-R2 complex. It was determined in the course of this study that R2 containing only Mn^{II} does not react with O_2 (not shown), whereas previous studies had established that the $Fe_2^{II/II}$-R2 complex reacts rapidly (7,10). The reaction of $Fe_2^{II/II}$-R2 results in development and decay of the absorption spectrum and sharp, isotropic, $g = 2.00$ EPR signal of the $Fe_2^{III/IV}$ cluster (7,

10). To minimize this undesired reaction, stopped-flow absorption and freeze-quench EPR experiments employed a three-fold excess of Mn over Fe. Mn^{II} (1.5 equiv relative to R2 monomer) was added to the metal-depleted R2 protein first, and the solution was incubated at ambient temperature (22 °C) to allow for binding. Fe^{II} (0.5 equiv) was then added slowly. This solution was loaded into the stopped-flow or freeze-quench apparatus. For preparation of the freeze-quenched sample for Mössbauer characterization of the Mn^{IV}/Fe^{IV}-R2 intermediate, a two-fold excess of Mn^{II} over Fe^{II} was employed. The divalent metal ions (1.0 equiv Mn^{II}, 0.5 equiv $^{57}Fe^{II}$) were pre-mixed before being added to the metal-depleted R2. The Mn^{II}/Fe^{II}-R2 solution was then loaded into the freeze-quench syringe.

Stopped-flow Absorption and Freeze-quench EPR and Mössbauer Experiments

The stopped-flow and freeze-quench apparatus and procedures and the EPR and Mössbauer spectrometers have been described (13). The magnitudes of the static magnetic fields for the low-field Mössbauer spectra were determined using a Digital Tesla meter (model 132D) with a Hall probe LPT 130-20S (Group3 Technologies Inc., Auckland, NZ). Details of reaction and spectroscopy conditions are provided in the appropriate figure legend or in the figure itself.

Simulation of the EPR and Mössbauer Spectra of Mn^{IV}/Fe^{IV}-R2

The simulations are based on the commonly used spin Hamiltonian formalism (14) and were carried out with respect to the total spin of the electronic ground state, $S_{Total} = 1/2$. For simulation of the EPR spectra, Equation 1 was used. The first term is the electron Zeeman effect and the second and third terms are the hyperfine couplings between the electron spin and the ^{55}Mn nuclear spin ($I = 5/2$) and between the electron spin and the ^{57}Fe nuclear spin ($I = 1/2$), respectively.

$$\widehat{\mathbf{H}}=\beta\,\mathbf{S}\bullet\mathbf{g}\bullet\mathbf{B}+\mathbf{S}\bullet\mathbf{A}_{\mathbf{Mn}}\bullet\mathbf{I}_{\mathbf{Mn}}+\mathbf{S}\bullet\mathbf{A}_{\mathbf{Fe}}\bullet\mathbf{I}_{\mathbf{Fe}} \quad (1)$$

The program SimFonia (Bruker, Billerica, MA) was used to simulate EPR spectra by the second-order-perturbation method for powder spectra. The full-matrix diagonalization program, SIM, which was written by Høgni Weihe (University of Copenhagen) (15), was used to simulate the spectra by an independent method to verify the parameters obtained with SimFonia. For simulation of the Mössbauer spectra, the program WMOSS (Web Research, Edina, MN) was used. All simulations were carried out with the assumption that the fluctuation rate of the electron spin is slow compared to the ^{57}Fe Larmor frequency. The first two terms of equation 1 were solved first with the parameters obtained from analysis of the EPR spectra. It was necessary to consider $\mathbf{A}_{Mn}$ explicitly, because it affects the splitting in the weak-field (B < ~150 mT) spectra. Coupling between the electron spin of the ground state, $S = 1/2$, and the ^{55}Mn nuclear spin, $I = 5/2$, leads to two states with spins $F = 2$ and $F = 3$ (with $\mathbf{F} = \mathbf{S} + \mathbf{I}$). For B > 150 mT, the electron Zeeman effect dominates the $\mathbf{S}.\mathbf{A}_{Mn}.\mathbf{I}$ term, the states are "pure" and characterized by the M_S [= ± 1/2] and M_I [= ± 1/2, ± 3/2, ± 5/2] quantum numbers (Figure S1), and the spin expectation values are at their maxima, $|\langle S\rangle| = 0.5$. With weaker applied fields, the electron Zeeman interaction and $\mathbf{A}_{Mn}$ are comparable, leading to mixing of the states. From the solution of the first two terms in eq 1, the spin expectation value, $\langle\mathbf{S}\rangle$, was calculated. Equation 2, in which all symbols have their usual meaning (14), was then used to compute the Mössbauer spectrum. All tensors were assumed to be collinear.

$$\widehat{\mathbf{H}}=\frac{eQV_{zz}}{12}\left[3\mathbf{I}_{\mathbf{Fe,z}}^2-I_{Fe}\left(I_{Fe}+1\right)+\eta\left(\mathbf{I}_{\mathbf{Fe,x}}^2-\mathbf{I}_{\mathbf{Fe,y}}^2\right)\right]+\langle\mathbf{S}\rangle\bullet\mathbf{A}_{\mathbf{Fe}}\bullet\mathbf{I}_{\mathbf{Fe}}-g_{n,Fe}\beta_{\mathbf{n}}\mathbf{B}\bullet\mathbf{I}_{\mathbf{Fe}} \quad (2)$$

RESULTS

Freeze-quench EPR evidence for accumulation of an oxidized Mn/Fe intermediate

The EPR spectrum of the O_2-reactive Mn^{II}/Fe^{II}-R2 complex, resolved as the difference of the spectra taken before and after exposure of the reactant solution to O_2 (Figure S2), exhibits a broad resonance centered at $g \sim 2$ that shows hyperfine coupling characteristic of an $I = 5/2$ ^{55}Mn nucleus. Optimal detection of this signal requires relatively low temperature and high power (e.g., 4.2 K and 20 mW, as in Figure S2). Spectra of samples freeze-quenched during the reaction of this complex with O_2 were recorded under less stringent conditions (14 K and 20 μW) to eliminate the contribution from the reactant complex. By subtracting the spectrum of the reactant solution under these conditions from the spectra of the freeze-quenched samples, the contribution of free Mn^{II} (resulting from the use of excess Mn^{II} in preparation of the reactant complex) was also removed. The time-dependent spectra (Figure 1A) illustrate that an intermediate with a sharp $g \sim 2$ EPR signal develops rapidly upon reaction with O_2 and then decays slowly. The spectrum of this intermediate has six lines separated by ~ 80 G that reflect hyperfine coupling to a single ^{55}Mn nucleus. When the intermediate is formed from Mn^{II}/Fe^{II}-R2 reactant containing ^{57}Fe, the sextet signal also shows hyperfine coupling to this $I = 1/2$ nucleus (compare the first and third spectra in Figure 1B). Simulation of these spectra (Figure 1B, second and fourth spectra) together with the Mössbauer spectra to extract electronic structural parameters (including the ^{55}Mn and ^{57}Fe hyperfine coupling tensors, $\mathbf{A}_{Mn}$ and $\mathbf{A}_{Fe}$) is presented below.

Kinetics of the reaction by stopped-flow absorption measurements

Accumulation of the Mn/Fe intermediate complex is also apparent in the time-dependent absorption spectra from the reaction (Figure 2A). An intense feature at ~ 390 nm develops rapidly (black, red and blue traces) and then decays slowly, leaving the spectrum of the Mn^{IV}/Fe^{III}-R2 product (green) (16). An overlay of the scaled intensities of the EPR spectra from the experiment of Figure 1A (Figure 1B, filled circles) with the absorbance-versus-time trace from the stopped-flow experiment with the same reaction conditions (Figure 1B, diamonds) illustrates that the $g \sim 2$ EPR signal and 390-nm absorption feature arise from the same intermediate. The kinetics of the intermediate were defined and the effects of variation of $[O_2]$ and inclusion of a reductant (ascorbate) were interrogated by additional stopped-flow experiments. Formation of the intermediate is kinetically first-order in $[O_2]$ (Figure 2B). The re-plot of the apparent first-order rate constant, obtained by fitting the equation for two parallel first-order reactions to the data,[2] versus $[O_2]$ gives a second-order rate constant (slope) of 13 (± 3) $mM^{-1}s^{-1}$ (Figure 2B, inset).

Formation of the Y• and $Fe_2^{III/III}$ cluster of a conventional class I RNR requires transfer of an "extra" electron to the buried cofactor during its reaction with O_2 (17-19). It has been shown that ascorbate can donate this electron (17,19). Similarly, the Mn^{IV}/Fe^{III} cofactor of active *Ct* R2 is three units more oxidized than the Mn^{II}/Fe^{II}-R2 complex, which reacts with the four-electron oxidant, O_2, to produce the active state (12,16). Thus, an extra electron is also required in activation of *Ct* R2. The ability of ascorbate to donate this electron and the timing and mechanism of donation were evaluated. Indeed, ascorbate accelerates decay of the intermediate in concentration-dependent fashion without affecting the kinetics of its formation (Figure 2C). The acceleration of its decay to the Mn^{IV}/Fe^{III} state by a reductant is consistent with its

[2]It is generally considered appropriate to invoke the pseudo-first-order approximation implicit in this fitting analysis only when one reactant is in 10–20-fold excess over the other. In these experiments, O_2 is in excess over the theoretical concentration of reactive Mn^{II}/Fe^{II}-R2 complex by a minimum of 2.3-fold and a maximum of 9.0-fold. However, within this range, the apparent first-order rate constant still behaves as a nearly linear function of the concentration of the excess reactant (see Figure S3) and the error introduced into the second-order rate constant by the approximation is small (~ 10%) in comparison with other sources (e.g., ~ 25% in the values of $[O_2]$).

assignment from the spectroscopic data as a Mn^{IV}/Fe^{IV} complex (*vide infra*). A plot of the observed first-order rate constant for decay versus [ascorbate] is hyperbolic (Figure 2C, inset), suggesting that a unimolecular step is rate-limiting for reduction of the Mn^{IV}/Fe^{IV} complex at high [ascorbate]. The nature of this step is discussed below.

Characterization of the intermediate by EPR and Mössbauer spectroscopy

The electronic structure of the intermediate was probed further by EPR and Mössbauer spectroscopies. Analysis of the data demonstrates that the intermediate has an $S = 1/2$ ground state as a consequence of antiferromagnetic coupling between the Mn^{IV} ($S_{Mn} = 3/2$) and high-spin Fe^{IV} ($S_{Fe} = 2$) ions.

As noted, the EPR spectrum of the intermediate prepared with ^{56}Fe exhibits six "packets" of intensity, due to hyperfine coupling with one ^{55}Mn. The second packet (at ~ 3210 G) is isotropic (i.e., all transitions are observed at the same magnetic field). The other five packets either are somewhat broadened or exhibit resolved features due to anisotropy of the **g**- and $\mathbf{A}_{Mn}$-tensors. The resolution of the features within the packets, especially for the fifth and sixth packets, permits determination of the **g**- and $\mathbf{A}_{Mn}$-tensors directly from simulation analysis (Table 1). $\mathbf{A}_{Mn}$ is nearly isotropic [(247, 216, 243) MHz], similar to $\mathbf{A}_{Mn}$ for the Mn^{IV} site of $Mn_2^{III/IV}$ catalase[3] [(235, 224, 252) MHz] (20) and as expected for a Mn^{IV} site (20,21). In simulating the EPR spectrum of the intermediate prepared with ^{57}Fe, the **g**- and $\mathbf{A}_{Mn}$-tensors determined from the spectrum of the intermediate containing ^{56}Fe were assumed and hyperfine coupling to the ^{57}Fe was then imposed. An isotropic $\mathbf{A}_{Fe}$-tensor was assumed first, but it became obvious that the quality of the simulation could be improved considerably with an anisotropic $\mathbf{A}_{Fe}$. By considering the EPR spectra together with the field-dependent Mössbauer spectra (*vide infra*), $\mathbf{A}_{Fe}$ was determined (Table 1).

The 4.2-K/53-mT Mössbauer spectra (Figure S4) of the Mn^{II}/Fe^{II}-R2 complex (top spectrum) and samples prepared by reacting this complex at 5 °C with O_2 for 0.090 s (second spectrum from top), 2.0 s (near the time of maximal accumulation of the intermediate; third spectrum from top) or 10 min (completion; bottom two spectra) before freezing illustrate the accumulation of the intermediate to a high level and its subsequent decay to the previously characterized Mn^{IV}/Fe^{III}-R2 product (16). Importantly, comparison of the spectra of the 0.09-s and 2-s samples shows that the dominant features in the latter spectrum develop with the same kinetics as for the $g \sim 2$ EPR signal and 390-nm absorption feature and are therefore associated with the same intermediate. Specifically, analysis of the spectrum of the 0.09-s sample suggests that ~40% of the intensity of the spectrum is attributable to the intermediate.

The 4.2-K/variable-field Mössbauer spectra of the 2-s sample are dominated (~70% of the absorption area) by features of the intermediate (Figure 3). Ideally, the spectral contributions of the minor species would be removed by subtraction of appropriate reference spectra in order to resolve the spectrum of the intermediate for detailed simulation analysis. However, in this case, even though the accumulation of the intermediate compares favorably with the best cases that we have encountered in previous studies, the multiplicity and unknown identities of the minor species make removal of their contributions impossible. The major "contaminant" is a high-spin Fe^{II} species of unknown identity.[4] Its presence is most clearly revealed in the weak-field ($B < 53$ mT) spectra by peaks at −0.2 mm/s and +2.8 mm/s (~17% intensity; Figure 3,

[3]The Mn^{IV} sites of the $Mn_2^{III/IV}$ cluster of catalase and the Mn^{IV}/Fe^{IV} intermediate in *Ct* R2 have the same spin projection factors, and therefore the magnitudes of the $\mathbf{A}_{Mn}$-tensors with respect to the total spin of the $S = 1/2$ ground state can be directly compared.

[4]Candidates for the Fe^{II} complex(es) are aqueous Fe^{II}, complexes in which the divalent metal is bound to R2 either in mononuclear fashion or in a homodinuclear or heterodinuclear cluster, or some combination of these. The Fe^{II}-associated features remaining in the spectrum of the 2-s sample are different from the spectrum of the reactant complex and thus cannot simply be removed by subtraction of this spectrum.

middle spectrum, blue line). The magnetic field dependence of the Fe^{II}-associated spectral component is unknown, precluding its removal. Fortunately, it is clear that, as expected for high-spin ($S = 2$) Fe^{II}, the Mössbauer features become broader and contribute little to the overall line-shape of the experimental spectrum of the 2-s sample with increasing field strengths. The remaining contaminants are predictable from the previously characterization of the product of the reaction (16), which showed that it contains ~80% Mn^{IV}/Fe^{III}-R2 and ~20% of the homodinuclear $Fe_2^{III/III}$ product. Thus, the iron in the 2-s sample not associated with the Mn^{IV}/Fe^{IV} intermediate and Fe^{II} contaminant should be distributed among the Mn^{IV}/Fe^{III} and $Fe_2^{III/III}$ products and the $Fe_2^{III/IV}$ precursor (**X**) to the latter product. Given the slow decay of both the Mn^{IV}/Fe^{IV} intermediate and **X**, only a small fraction should be in the form of the products at a reaction time of 2 s. Indeed, whereas the experimental spectra can accommodate a small contribution from the product species (≤ 9% total), their contribution could be much less or even negligible. The spectra do reveal the presence of a small quantity of the $Fe_2^{III/IV}$ complex.[5] In particular, two features of **X** are nearly fully resolved in the 13-mT spectrum and can be used to estimate the contribution from the complex (~11%; Figure 3, bottom spectrum, red line). In addition, the highest-energy lines of the sub-spectra of the Fe^{IV} and Fe^{III} sites are coincident at 3.7 mm/s in the 8-T spectrum, resulting in a more intense line that reveals the presence of the complex (Figure 3, top spectrum, red line).

Despite this heterogeneity, the predominance of the Mn^{IV}/Fe^{IV} intermediate makes the positions and shapes of its features sufficiently clear for simulations to be used to extract spectroscopic parameters (Table 1 and Figure 3, solid black lines). In particular, the contributions of species with integer-electron-spin ground states (Fe^{II} species and the Mn^{IV}/Fe^{III} and $Fe_2^{III/III}$ products) are canceled in field orientation dependent spectra (53 mT ∥ − 53 mT ⊥) and the contributions of the species with half-integer-spin (the Mn^{IV}/Fe^{IV} and $Fe_2^{III/IV}$ intermediates) are resolved (14). The contribution from the $Fe_2^{III/IV}$ intermediate (red line) is small compared to that of the Mn^{IV}/Fe^{IV} intermediate (black line). This difference spectrum provides constraints on the parameters of the Mn^{IV}/Fe^{IV} intermediate, in particular the isomer shift (δ). Because δ must be determined from magnetically split spectra,[6] the uncertainty in this crucial parameter is fairly large (0.06 mm/s). Nevertheless, even with the large uncertainty, the value of δ (0.17 ± 0.06 mm/s) indicates that the intermediate has an Fe^{IV} site. Indeed, the center of the range is essentially identical with δ of the $Fe_2^{IV/IV}$ complex, **Q**, in the reaction of soluble methane monooxygenase (22,23).

The hyperfine tensor for the Fe^{IV} site with respect to the total spin of the ground state ($S = 1/2$), $\mathbf{A}_{Fe}$, determines the splitting in the spectra and is given by the product of the intrinsic hyperfine tensor, $\mathbf{a}_{Fe}$, and the spin projection factor, c_{Fe} (Equation 3) (24).

$$\mathbf{A}_{Fe} = \mathbf{c}_{Fe} \cdot \mathbf{a}_{Fe} \tag{3}$$

The components of $\mathbf{A}_{Fe}$ are negative, as revealed by the decrease of the overall splitting with increasing applied magnetic field (e.g., compare the 53-mT, 4-T, and 8-T spectra in Figure 3) (25). The components of the intrinsic hyperfine tensor for iron, $\mathbf{a}_{Fe}$, are negative. Thus, c_{Fe} must be positive. A positive value of c_{Fe} requires that $S_{Fe} > S_{Mn}$ (3/2). The Fe^{IV} site must therefore be in the high-spin configuration ($S_{Fe} = 2$). For this spin system, $c_{Fe} = 2$ for the $S = 1/2$ ground state, giving $\mathbf{a}_{Fe} = (-28.0, -29.7, -20.3)$ MHz. These values are almost identical

[5]The 4.2-K/53-mT Mössbauer features of the $Fe_2^{III/IV}$ cluster, **X**, of *Ct* R2, which accumulates to a large amount in the reaction of the Fe_2-form of *Ct* R2 are almost identical to those of **X** from *E. coli* R2 (unpublished results). Therefore, we used the published parameters of *E. coli* **X** (26) to simulate **X** of *Ct* R2.

[6]The standard tactic of raising the temperature to make the electronic fluctuation rapid with respect to the nuclear precession frequency and thereby collapse the magnetic spectrum into a quadrupole doublet for more accurate determination of δ and ΔE_Q failed. The 120 K/zero-field spectrum is very broad and featureless, implying that the fluctuation rate of the electronic states is comparable to the ^{57}Fe Larmor frequency (the intermediate relaxation regime) at this temperature.

to those of the high-spin Fe^{IV} site of cluster **X** in *E. coli* R2 [$\mathbf{a}_{Fe}$ = (−27.6, −27.6, − 20.6) MHz] (26), consistent with the assignment of the Fe site of the *Ct* R2 intermediate as high-spin Fe^{IV}.

The **g**-tensor of the $S = 1/2$ ground state, given by Equation 4 (24), is nearly isotropic as a result of relatively small anisotropy of $\mathbf{g}_{Fe}$ and $\mathbf{g}_{Mn}$, as was observed before for Mn^{IV} and high-spin Fe^{IV} species (20, 26).

$$\mathbf{g}_{S=1/2} = 2\,\mathbf{g}_{Fe} - \mathbf{g}_{Mn} \quad (4)$$

Comparison of the low-field spectra clearly illustrates the perturbation associated with the hyperfine coupling to the $I = 5/2$ ^{55}Mn nucleus, which is comparable in magnitude to the electron Zeeman term in weak fields. For example, at a field of 13 mT (Figure 3, bottom spectrum), the absolute magnitude of the internal magnetic field [given by $-\langle \mathbf{S} \rangle \bullet (\mathbf{A}/g_N\beta_N)_{Fe}$] is smaller for some of the states as a consequence of sub-saturating values of $\langle \mathbf{S} \rangle$ (see Figure S1 for plots of the field-dependence of the spin expectation values), resulting in reduced splitting and greater intensity in the center of the spectrum. As the field is increased in the 0 – 150 mT regime, $\langle \mathbf{S} \rangle$ and the magnetic splitting increase (compare to the 53-mT ∥ spectrum; Figure 3, middle). With much greater fields (B > 150 mT), splitting decreases again (compare 53-mT ∥ spectrum to 8-T spectrum) because for the ground state the applied field opposes the already saturated internal field from the electron spin.

DISCUSSION

The stopped-flow absorption and freeze-quench EPR and Mössbauer data thus establish that the active Mn^{IV}/Fe^{III} cofactor of *Ct* RNR forms via a Mn^{IV}/Fe^{IV} intermediate that decays by reduction of the Fe^{IV} site (Scheme 1, top). The Mn^{IV} ($S_{Mn} = 3/2$) and high-spin Fe^{IV} ($S_{Fe} = 2$) sites of the intermediate couple antiferromagnetically to yield an $S = 1/2$ ground state. Whereas a Mn^{IV}/Fe^{III} complex has been reported (27), the *Ct* R2 intermediate is, to our knowledge, the first example of a Mn^{IV}/Fe^{IV} complex. In view of the X-ray crystal structure of the (presumptively) $Fe_2^{III/III}$ form of the *Ct* R2 protein by Högbom, et al. (7), which suggested a *bis*-(μ-hydroxo)-dimetal core, and previous studies suggesting formation of a $(\mu\text{-}O)_2\text{-}Fe_2^{IV/IV}$ complex, **Q**, in the catalytic cycle of soluble methane monooxygenase (28), we consider it very likely that the Mn^{IV}/Fe^{IV} intermediate also has this $[M_2O_2(H)_n]^{(4+n)+}$ "diamond core" structure. Its half-integer ($S = 1/2$) electron-spin ground state, which contrasts with the $S = 0$ ground state of **Q**, and heterodinuclear rather than homodinuclear nature should afford unique opportunities to test this hypothesis and probe details of the core structure by electron-nuclear double resonance (ENDOR) and X-ray absorption experiments.

Q and the Y•-generating $Fe_2^{III/IV}$ intermediate, **X**, form from the corresponding μ-peroxo-$Fe_2^{III/III}$ intermediates in methane monooxygenase (29) and conventional RNR-R2 proteins (29,30), respectively. However, no $Fe_2^{IV/IV}$ complex has ever been detected in an R2 protein, either because O-O cleavage occurs reductively or because the $Fe_2^{IV/IV}$ complex is reduced too rapidly to accumulate. In the best-studied R2 reaction, in *E. coli* R2, tryptophan (W) 48 near the protein's surface is the proximal electron source for this step, and the resultant W48 cation radical is readily reduced by a variety of compounds (Fe^{II}_{aq}, ascorbate, thiols) (Scheme 1, bottom) (31). A radical of the corresponding W residue in *Ct* R2, W51, has been detected during O_2 activation by the $Fe_2^{II/II}$ forms of variants of *Ct* R2 (W. Jiang, L. Saleh, J. M. Bollinger, Jr., unpublished observations), proving that this residue can function equivalently in the class Ic R2 and could, in principle, rapidly reduce the Mn^{IV}/Fe^{IV} cluster to limit its accumulation. Apparently, changes accompanying replacement of one Fe by Mn (e.g., of the mechanistic pathway or reduction potentials of constituent complexes), structural adjustments to the cluster site (e.g., the presence of E89 in *Ct* R2 in place of the D84 found in *E. coli* R2),

or both allow the IV/IV state to build up uniquely in the *Ct* R2 protein. Nevertheless, the "saturation" of the observed rate constant in Figure 2C suggests that reduction of the Mn^{IV}/Fe^{IV} complex by ascorbate might also take place by a two-step mechanism, with the first step being the oxidation of W51 (or perhaps another residue). A rate-constant of $0.7 \pm 0.1\ s^{-1}$, the asymptotic value of k_{obs} for decay of the intermediate, for the first step in this hypothetical electron-shuttling mechanism would rationalize the saturation of the decay rate constant at this value. This speculation should be testable by use of alternative reductants and variant R2 proteins.

It remains to be seen whether the Mn^{IV}/Fe^{IV} intermediate, like **Q** and **X**, forms from a (μ-peroxo)-$M_2^{III/III}$ intermediate. The stopped-flow and freeze-quench EPR data provide no evidence for the accumulation of such a complex. Thus, as in *E. coli* R2, it might prove necessary to perturb the reaction kinetics (e.g., by replacement of a ligand, as in the D84E substitution in *E. coli* R2 that was shown to stabilize the peroxide intermediate (32)) to permit accumulation of a peroxide precursor to the Mn^{IV}/Fe^{IV} intermediate.

Supplementary Material

Refer to Web version on PubMed Central for supplementary material.

REFERENCES

1. Stubbe J. Di-iron-tyrosyl radical ribonucleotide reductases. Curr. Opin. Chem. Biol 2003;7:183–188. [PubMed: 12714050]
2. Stubbe J, Nocera DG, Yee CS, Chang MCY. Radical initiation in the Class I ribonucleotide reductase: long-range proton-coupled electron transfer? Chem. Rev 2003;103:2167–2202. [PubMed: 12797828]
3. Nordlund P, Reichard P. Ribonucleotide reductases. Annu. Rev. Biochem 2006;75:681–706. [PubMed: 16756507]
4. Licht S, Gerfen GJ, Stubbe J. Thiyl radicals in ribonucleotide reductases. Science 1996;271:477–481. [PubMed: 8560260]
5. Mao SS, Yu GX, Chalfoun D, Stubbe J. Characterization of C439SR1, a mutant of *Escherichia coli* ribonucleotide diphosphate reductase: evidence that C439 is a residue essential for nucleotide reduction and C439SR1 is a protein possessing novel thioredoxin-like activity. Biochemistry 1992;31:9752–9759. [PubMed: 1390751]
6. Roshick C, Iliffe-Lee ER, McClarty G. Cloning and Characterization of Ribonucleotide Reductase from *Chlamydia trachomatis*. J. Biol. Chem 2000;275:38111–38119. [PubMed: 10984489]
7. Högbom M, Stenmark P, Voevodskaya N, McClarty G, Gräslund A, Nordlund P. The radical site in Chlamydial ribonucleotide reductase defines a new R2 subclass. Science 2004;305:245–248. [PubMed: 15247479]
8. Bollinger JM Jr. Edmondson DE, Huynh BH, Filley J, Norton JR, Stubbe J. Mechanism of assembly of the tyrosyl radical-dinuclear iron cluster cofactor of ribonucleotide reductase. Science 1991;253:292–298. [PubMed: 1650033]
9. Yun D, Krebs C, Gupta GP, Iwig DF, Huynh BH, Bollinger JM Jr. Facile electron transfer during formation of cluster X and kinetic competence of X for tyrosyl radical production in protein R2 of ribonucleotide reductase from mouse. Biochemistry 2002;41:981–990. [PubMed: 11790122]
10. Voevodskaya N, Lendzian F, Gräslund A. A stable Fe^{III}-Fe^{IV} replacement of tyrosyl radical in a class I ribonucleotide reductase. Biochem. Biophys. Res. Commun 2005;330:1213–1216. [PubMed: 15823572]
11. Voevodskaya N, Narvaez AJ, Domkin V, Torrents E, Thelander L, Gräslund A. Chlamydial ribonucleotide reductase: tyrosyl radical function in catalysis replaced by the Fe^{III}-Fe^{IV} cluster. Proc. Natl. Acad. Sci. U.S.A 2006;103:9850–9854. [PubMed: 16777966]
12. Jiang W, Yun D, Saleh L, Barr EW, Xing G, Hoffart LM, Maslak M-A, Krebs C, Bollinger JM Jr. A Manganese(IV)/Iron(III) Cofactor in *Chlamydia trachomatis* Ribonucleotide Reductase. Science 2007;316:1188–1191. [PubMed: 17525338]

13. Price JC, Barr EW, Tirupati B, Bollinger JM Jr. Krebs C. The First Direct Characterization of a High-Valent Iron Intermediate in the Reaction of an α-Ketoglutarate-Dependent Dioxygenase: A High-Spin Fe(IV) Complex in Taurine/α-Ketoglutarate Dioxygenase (TauD) from *Escherichia coli*. Biochemistry 2003;42:7497–7508. [PubMed: 12809506]
14. Münck, E. Physical Methods in Bioinorganic Chemistry. Que, L., Jr., editor. University Science Books; Sausalito, CA: 2000. p. 287-319.
15. Glerup J, Weihe H. Magnetic Susceptibility and EPR Spectra of (μ-Hydroxo)bis [pentaamminechromium(III)] Chloride Monohydrate. Inorg. Chem 1997;36:2816–2819. [PubMed: 11669916]
16. Jiang W, Bollinger JM Jr. Krebs C. The active form of *Chlamydia trachomatis* ribonucleotide reductase R2 protein contains a heterodinuclear Mn(IV)/Fe(III) cluster with $S = 1$ ground state. J. Am. Chem. Soc. 2007published on the web on May 27, 2007
17. Ochiai E, Mann GJ, Gräslund A, Thelander L. Tyrosyl free radical formation in the small subunit of mouse ribonucleotide reductase. J. Biol. Chem 1990;265:15758–15761. [PubMed: 2203785]
18. Elgren TE, Lynch JB, Juarez-Garcia C, Münck E, Sjöberg BM, Que L Jr. Electron transfer associated with oxygen activation in the B2 protein of ribonucleotide reductase from Escherichia coli. J. Biol. Chem 1991;266:19265–19268. [PubMed: 1918044]
19. Bollinger JM Jr. Tong WH, Ravi N, Huynh BH, Edmonson DE, Stubbe J. Mechanism of Assembly of the Tyrosyl Radical-Diiron(III) Cofactor of E. coli Ribonucleotide Reductase. 2. Kinetics of The Excess Fe2+ Reaction by Optical, EPR, and Moessbauer Spectroscopies. J. Am. Chem. Soc 1994;116:8015–8023.
20. Zheng M, Khangulov SV, Dismukes GC, Barynin VV. Electronic structure of dimanganese(II,III) and dimanganese(III,IV) complexes and dimanganese catalase enzyme: a general EPR spectral simulation approach. Inorg. Chem 1994;33:382–387.
21. Sinnecker S, Neese F, Lubitz W. Dimanganese catalase-spectroscopic parameters from broken-symmetry density functional theory of the superoxidized Mn^{III}/Mn^{IV} state. J. Biol. Inorg. Chem 2005;10:231–238. [PubMed: 15830216]
22. Lee S-K, Fox BG, Froland WA, Lipscomb JD, Münck E. A transient intermediate of the methane monooxygenase catalytic cycle containing an $Fe^{IV}Fe^{IV}$ cluster. J. Am. Chem. Soc 1993;115:6450–6451.
23. Liu KE, Wang D, Huynh BH, Edmondson DE, Salifoglou A, Lippard SJ. Spectroscopic detection of intermediates in the reaction of dioxygen with the reduced methane monooxygenase/hydroxylase from *Methylococcus capsulatus* (Bath). J. Am. Chem. Soc 1994;116:7465–7466.
24. Bencini, A.; Gatteschi, D. EPR of exchange coupled systems. Springer; Berlin, Germany: 1990.
25. Krebs C, Price JC, Baldwin J, Saleh L, Green MT, Bollinger JM Jr. Rapid Freeze-Quench ^{57}Fe Mössbauer Spectroscopy: Monitoring Changes of an Iron-Containing Active Site during a Biochemical Reaction. Inorg. Chem 2005;44:742–757. [PubMed: 15859243]
26. Sturgeon BE, Burdi D, Chen S, Huynh BH, Edmondson DE, Stubbe J, Hoffman BM. Reconsideration of **X**, the diiron intermediate formed during cofactor assembly in *E. coli* ribonucleotide reductase. J. Am. Chem. Soc 1996;118:7551–7557.
27. Hotzelmann R, Wieghardt K, Flörke U, Haupt HJ, Weatherburn DC, Bonvoisin J, Blondin G, Girerd JJ. Spin exchange coupling in asymmetric heterodinuclear complexes containing the μ-oxo-*bis*(μ-acetato)dimetal core. J. Am. Chem. Soc 1992;114:1681–1696.
28. Shu L, Nesheim JC, Kauffmann KE, Münck E, Lipscomb JD, Que L Jr. An $Fe_2^{IV}O_2$ diamond core structure for the key intermediate **Q** of methane monooxygenase. Science 1997;275:515–518. [PubMed: 8999792]
29. Tong WH, Chen S, Lloyd SG, Edmondson DE, Huynh BH, Stubbe J. Mechanism of assembly of the diferric cluster-tyrosyl radical cofactor of *Escherichia coli* ribonucleotide reductase from the diferrous form of the R2 subunit. J. Am. Chem. Soc 1996;118:2107–2108.
30. Yun D, Garcia-Serres R, Chicalese BM, An YH, Huynh BH, Bollinger JM Jr. (μ-1,2-Peroxo)diiron (III/III) Complex as a Precursor to the Diiron(III/IV) Intermediate X in the Assembly of the Iron-Radical Cofactor of Ribonucleotide Reductase from Mouse. Biochemistry 2007;46:1925–1932. [PubMed: 17256972]

31. Baldwin J, Krebs C, Ley BA, Edmondson DE, Huynh BH, Bollinger JM Jr. Mechanism of Rapid Electron Transfer during Oxygen Activation in the R2 Subunit of *Escherichia coli* Ribonucleotide Reductase. 1. Evidence for a Transient Tryptophan Radical. J. Am. Chem. Soc 2000;122:12195–12206.

32. Bollinger JM Jr. Krebs C, Vicol A, Chen S, Ley BA, Edmondson DE, Huynh BH. Engineering the diiron site of *Escherichia coli* ribonucleotide reductase protein R2 to accumulate an intermediate similar to H_{peroxo}, the putative peroxodiiron(III) complex from the methane monooxygenase catalytic cycle. J. Am. Chem. Soc 1998;120:1094–1095.

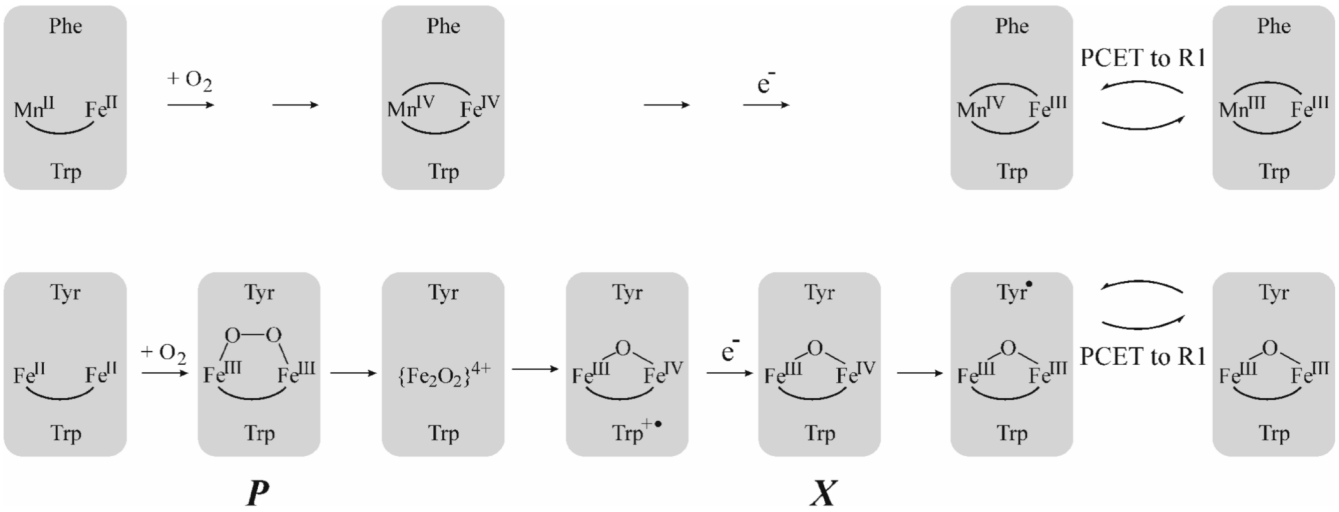

Scheme 1.
Mechanisms of the R2 activation reactions in *Ct* R2 (top) and *E. coli* R2 (bottom).

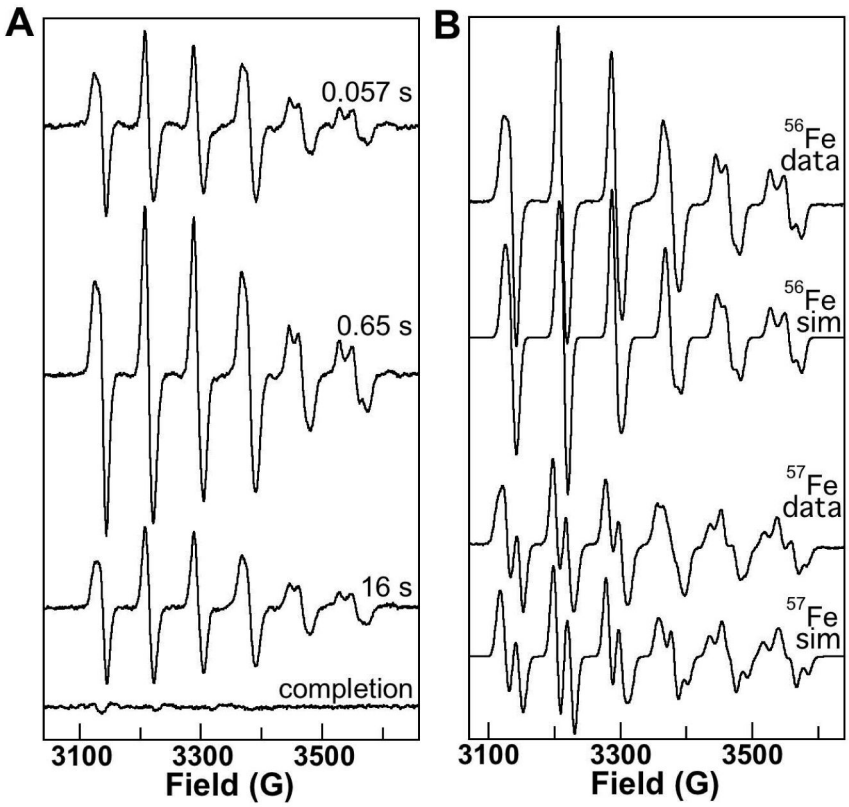

Figure 1.

X-band EPR spectra at 14.0 (± 0.2) K of the Mn^{IV}/Fe^{IV} intermediate in activation of *Ct* R2. **A**: Spectra of samples freeze-quenched at various reaction times (indicated on the figure) after mixing at 5 °C of an O_2-free solution of Mn^{II}/Fe^{II}-R2 (0.40 mM R2 monomer, 0.5 equiv Fe, 1.5 equiv Mn) with an equal volume of O_2-saturated buffer. The spectrum of the recovered product (completion) sample has been scaled to account for the fact that it was manually frozen rather than being freeze-quenched (× 0.6, the "packing factor" typical of freeze-quenched samples). In addition, the appropriately scaled spectrum of the reactant sample (× 0.5 because it wasn't diluted and × 0.6 because it was manually frozen) was subtracted from the experimental spectrum of each sample to generate the spectra shown. **B**: spectra of samples prepared by manual mixing of an O_2-free solution of Mn^{II}/Fe^{II}-R2 (3.0 mM R2 monomer, 0.75 equiv of each metal ion) at ambient temperature (22 ± 2 °C) with 9 equivalent volumes of O_2-saturated buffer and freezing after 20 ± 2 s. The first and third traces are the experimental spectra of the samples prepared with ^{56}Fe and ^{57}Fe, respectively. Spectrometer conditions were: microwave frequency, 9.45 GHz; microwave power, 20 μW; modulation frequency, 100 kHz; modulation amplitude, 10 G; scan time, 167 s; time constant, 167 ms. The second and fourth traces are simulations of the experimental spectra generated as described in Material and Methods with the **g**, $\mathbf{A}_{Mn}$, and $\mathbf{A}_{Fe}$ tensors given in Table 1.

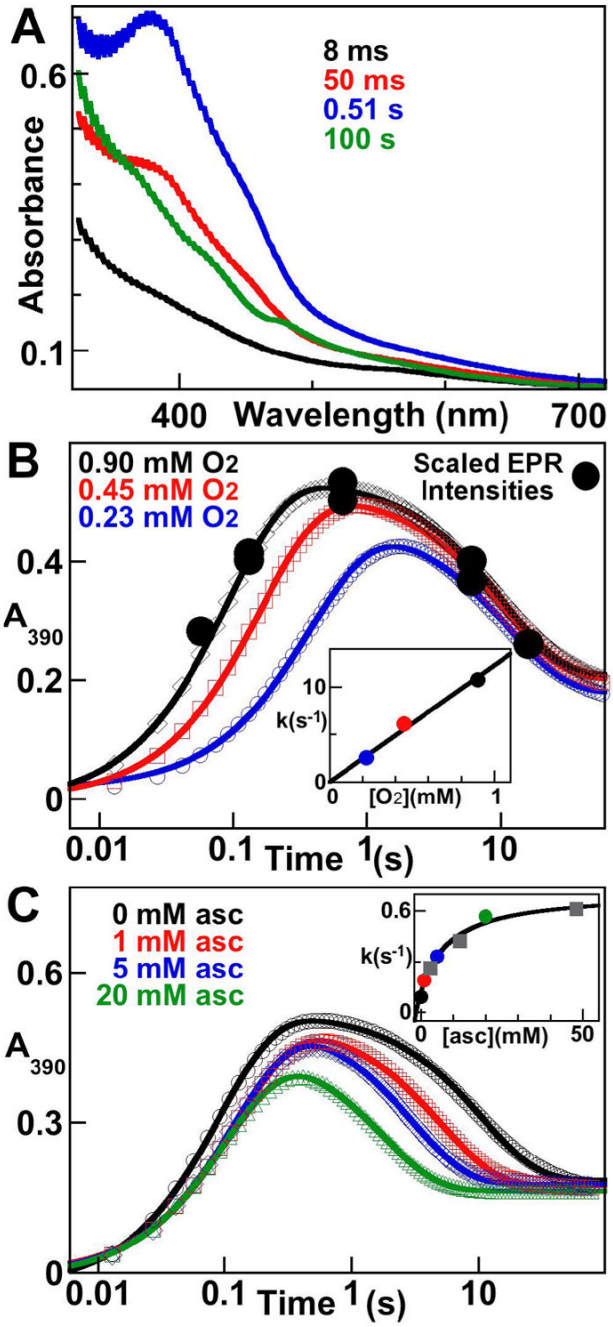

Figure 2.

Kinetics of the activation of *Ct* R2 by stopped-flow absorption spectroscopy. **A**: spectra acquired at the indicated reaction times after mixing at 5 °C of an O_2-free solution of Mn^{II}/Fe^{II}-R2 (0.40 mM R2 monomer, 0.5 equiv Fe, 1.5 equiv Mn) with an equal volume of O_2-saturated buffer. **B**: dependence of the kinetics of the reaction on [O_2]. An equivalent Mn^{II}/Fe^{II}-R2 solution was mixed with 100% (black), 50% (red), or 25% (blue) O_2-saturated buffer. The black circles are the EPR signal intensities from the experiment of Figure 1A (which had identical reaction conditions) scaled for direct comparison to the absorbance changes. The inset shows the apparent first-order rate constant for the formation phase of the reaction (obtained by fitting a "double-exponential" equation to the data[2]) versus [O_2], which gives a second order

rate-constant (slope) of 12 (± 3) $mM^{-1}s^{-1}$. **C**: Dependence of the kinetics on the concentration of ascorbate. The otherwise-equivalent Mn^{II}/Fe^{II}-R2 reactant solution, which contained ascorbate at a concentration sufficient to give the indicated [ascorbate] after mixing, was mixed with 100% O_2-saturated buffer. The inset shows the apparent first-order rate constant for the decay phase versus [ascorbate], which gives a limiting reduction rate constant (asymptote of hyperbolic fit) of 0.7 (± 0.1) s^{-1}.

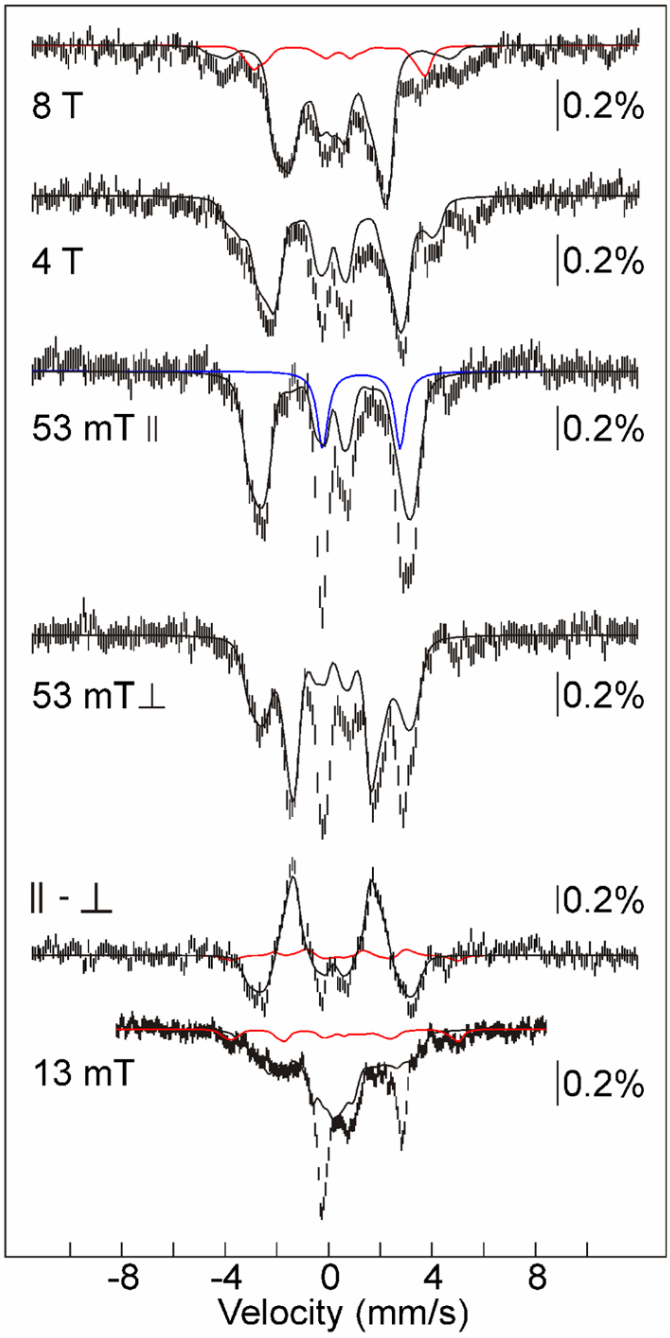

Figure 3.

4.2-K Mössbauer spectra in varying magnetic fields (as indicated on the spectra) of a sample containing primarily the Mn^{IV}/Fe^{IV} intermediate. The sample was prepared by mixing an O_2-free solution of Mn^{II}/Fe^{II}-R2 (3.0 mM R2 monomer, 0.5 equiv Fe and 1.0 equiv Mn) at 5 °C with an equal volume of O_2-saturated buffer and freeze-quenching at a reaction time of 2 s. Unless otherwise noted, the field was parallel to the γ-beam. The solid black lines plotted over the spectra are simulations of the spectra of the Mn^{IV}/Fe^{IV}-R2 intermediate as described in Materials and Methods with the parameters given in Table 1. They are scaled to account for 70% of the total intensity. The red lines are a simulation of the spectrum of the $Fe_2^{III/IV}$ complex (11% of total intensity) with the published parameters (26), and the blue line is a quadrupole

doublet with δ = 1.3 mm/s and ΔE_Q = 3.0 mm/s to illustrate the contribution from the Fe^{II} component of the sample (17% of total intensity).

Table 1

Spin-Hamiltonian parameters of the Mn^{IV}/Fe^{IV}-R2 intermediate.

Parameter	**Mn^{IV}/Fe^{IV}*Ct*-R2**	
g	**2.017, 2.030, 2.027**	
	Fe^{IV} site	**Mn^{IV} site**
A (MHz)	(−55.9, −59.3, −40.5)[a]	(247, 216, 243)
δ(mm/s)	0.17 (6)	-
ΔE_Q (mm/s)	−0.75	-
η	−10	-

[a] Sign determined from Mössbauer spectroscopy